This is the post-print (i.e. final draft post-refereeing) of the publication.
The final publication is available at Elsevier via http://dx.doi.org/10.1016/j.ceramint.2016.08.066

Effect of lanthanide doping on structural, microstructural and functional properties of $K_{0.5}Na_{0.5}NbO_3$ lead-free piezoceramics

X.Vendrell[1*], J.E. García[2], E. Cerdeiras[1], D.A. Ochoa[2], F. Rubio-Marcos[3], J. F. Fernández[3], L.Mestres[1]

[1] *Departament de Química Inorgànica i Orgànica, Secció Química Inorgànica, Universitat de Barcelona, 08028 Barcelona, Spain.*

[2] *Department of Physics, Universitat Politècnica de Catalunya, 08034 Barcelona, Spain.*

[3] *Electroceramic Department, Instituto de Cerámica y Vidrio, CSIC, 28049 Madrid, Spain.*

Abstract

Lanthanides-doped $K_{0.5}Na_{0.5}NbO_3$ (KNN) lead-free piezoelectric ceramics are prepared by conventional solid-state reaction. The effects of lanthanum concentration and the lanthanide type on the structure, microstructure and ferro-piezoelectric properties are evaluated. Ln^{3+} doping has a slight effect on the structure, but greatly inhibits the grain growth. Moreover, a decrease in the Curie temperature and an increase in the dielectric constant values are observed when doping. Large amounts of lanthanum induce a diffuse phase transition and an increase of the dielectric losses. The piezoelectric properties are greatly improved when doping with small amounts of dopants. As the ionic radii of the lanthanide is reduced, the piezoelectric properties of the ceramics are increased, the Eu^{3+}-doped ceramics show an increase of 29% of the piezoelectric coefficient d_{33} with respect to pure KNN. The results show that low concentrations of lanthanides improve significantly the functional properties of KNN lead-free piezoceramics. Doping with lanthanides should be taken into consideration in some other compositions based on KNN.

Keywords: Lead-free piezoceramics, Donor doping, Piezoelectric properties, $(K,Na)NbO_3$

*Dr. Xavier Vendrell
xavier.vendrell@ub.edu
Telf: +34 934 021 270
Fax: +34 934 907 725

1. Introduction

Piezoelectric materials are currently used in a wide range of applications, including motors, printing machines, micropositioning machines, atomic force microscopes and filters in mobile phones [1,2]. Owing to their effective piezoelectric coefficients, high dielectric permittivity, and high coupling factors, lead zirconate titanate-based materials (PZT) are the most commonly used piezoelectric ceramics [3].

The main disadvantage of lead-based piezoceramics is that they have highly toxic levels of lead. The high volatility of lead particularly during the heating steps of the ceramic preparation process causes lead to be released into the environment. Indeed, it is widely reported that even low levels of lead exposure can have numerous adverse effects on human health and the environment [4,5]. As a result, in 2003, the European Union opted to officially class lead zirconate titanate as a hazardous substance [6]. Nevertheless, as there are no lead-free replacements for lead-based piezoeramics, these materials are exempt from a ban on its use. However, it is important to note that this decision is reviewed periodically.

In recent years, extensive research has focused on the development of alternative lead-free piezoelectric materials to substitute the use of lead-based piezoceramics. Therefore, new piezoelectric ceramics such as bismuth titanates, alkali niobates, and other systems in which a morphotropic phase boundary (MPB) occurs [7–9] are being investigated for more than a decade to achieve new high performance lead-free piezoelectric ceramics. In this years, much attention has been given to $(K_{0.5}Na_{0.5})NbO_3$ (KNN)-based ceramics as a result of the breakthrough made by Saito et al. [10], where exceptionally high piezoelectric properties (~416 pC/N) in a KNN-based system prepared by a complex processing method were reported. However, it is very difficult to obtain dense and well-sintered KNN ceramics using a low cost, ordinary sintering process because of the high volatility of alkaline metals at high temperatures. Sintering aids such as CuO, SnO_2, ZnO or MnO_2 may improve sinterability and modify the dielectric and piezoelectric behaviour KNN-based ceramics [11–15].

The modified KNN ceramics seem to be a suitable substitute for lead-based materials. In a previous study we have demonstrated that the densification of KNN ceramics, as well as the dielectric and piezoelectric properties can be improved by doping with low amounts of acceptor dopants [16]. Therefore, doping is a very active research field in order to improve the functional properties of these materials. It is well known that donor doping is an effective approach to improve the piezoelectric properties of piezoelectric materials [17,18]. Moreover, lanthanide oxides, have been used as donor dopants or additives in PZT-based [19] or $BaTiO_3$-based [20] ceramics. However, in KNN-based ceramics it has not been extensively studied the effect of lanthanides as donor dopants. In fact, only a few authors have reported the effect of lanthanides doping, but usually with contradictory results [21–23]. Furthermore, the photoluminescence effect has also been determined in Pr^{3+} doped KNN ceramics [24], although the dielectric and piezoelectric properties were not reported. Hence, this work aims to prepare lanthanide-doped KNN ceramics by a simple and reproducible solid-state reaction method, and to study the influence of the lanthanum concentration and the type of lanthanide in the functional properties of KNN ceramics.

2. Experimental

The $(K_{0.5}Na_{0.5})_{1-3x}La_xNbO_3$ compositions with x = 0.0, 0.0025, 0.005, 0.0075, 0.01, 0.03 and 0.05, hereafter abbreviated as KNN:xLa and the $(K_{0.5}Na_{0.5})_{1-3x}Ln_xNbO_3$ compositions with x = 0.005, being Ln = La, Pr, Nd, Sm and Eu, abbreviated as KNN:Ln, were synthesized by conventional solid-state reaction. The raw materials of analytical grade used in this study were K_2CO_3 (99%), Na_2CO_3 (99.5%), Nb_2O_5 (99.9%), La_2O_3 (≥ 99.98%), Pr_6O_{11} (≥ 99.9%), Nd_2O_3 (99.9%), Sm_2O_3 (99.9%) and Eu_2O_3 (99.9%). Special care of the reagents was taken; each reagent was milled separately for achieving a uniform distribution of the particle size. After separate milling, the powders were weighed and mixed by ball milling using Y_2O_3-stabilized ZrO_2 balls in absolute ethanol medium for 3 h, then dried and calcined at 700 ºC for 2 h. The calcined powders were then milled again and pressed at 450 MPa into 7 mm diameter pellets and sintered in air, without a binder, at 1125 ºC for 2 h. Care was taken to ensure that a high

alkaline element pressure is maintained during the process by surrounding the pellets with powder of the same composition, and the pellets were deposited on platinum foils to avoid reaction with alumina boats. All as-sintered ceramics showed relative densities over 95% measured by Archimedes method.

X-ray diffractograms were recorded at room temperature on a PNAalytical X'Pert PRO MPD with Cu $K\alpha_1$ radiation. The patterns were recorded over the angular range 20-70º (2θ) with a step size of 0.017º and a time per step of 50 second, operated at 45 kV and 40 mA. The cell parameters and their evolution were refined by a LeBail fitting procedure as implemented in the Fullprof suite [25]. The Raman scattering spectra were obtained on a Jobin-Yvon Labram HR 800 (Horiba) spectrometer with an Ar excitation wavelength of 532 nm. Microstructure was evaluated using a Field Emission Scanning Electron Microscope, FE-SEM (JEOL JSM-7001F), equipped with Energy Dispersive Spectroscopy (EDS). Samples for transmission electron microscopy (TEM) were prepared from powders of the KNN-based ceramics suspended and ultrasonically dispersed in butanol. One drop of the suspension was placed on a copper grid coated by a holey carbon film. Selected-area electron diffraction and high-resolution TEM (HRTEM) experiments were performed using a JEOL 3000F microscope with a resolution limit of ≈1.1 Å. HRTEM images were recorded with an objective aperture of 70 μm centered on a sample spot within the diffraction pattern area. Fast Fourier transforms (FFTs) of the HRTEM images were carried out to reveal the periodic image contents using *Digital Micrograph* package [26]. The experimental HRTEM images were also compared to a simulated images using *MacTempas* software [27]. Such computations were performed using information from the structural parameters and microstructural parameters such as the microscope operating voltage (300 kV), the spherical aberration coefficient (0.6 mm), and the specimen parameters such as the zone axis and thickness. The defocus (f) and sample thickness (t) parameters were optimized by assessing the agreement between the model and data, leading to values of f = -400 Å and t = 40 Å.

For electrical characterization, the pellets were coated with silver paint on their upper and lower surfaces. The impedance spectroscopy technique was used to obtain the permittivity of the studied materials as a function of temperature and frequency. Admittance values were measured using an impedance analyzer, HP4192A, in the frequency range 100 Hz-1 MHz. A programmable furnace was used to examine the temperature dependence of permittivity from room temperature (RT) to 500 ºC. The ferroelectric hysteresis loops were recorded using a modified Sawyer-Tower circuit. The samples were poled in silicon oil at 80 ºC for 30 minutes under a 30 kV/cm DC electric field. Subsequently, the longitudinal piezoelectric coefficient was measured using a piezo-d_{33} meter (YE2730A, APC International) at RT. The piezoelectric constant d_{31} and the electromechanical coupling factor k_p were determined at RT by the resonance/antiresonance method on the basis of the IEEE standards.

3. Results and discussion

3.1. Structural characterization

Fig. 1(a) displays the XRD patterns of the KNN:xLa ceramics. A single phase is obtained for most of the prepared ceramics. Only when the ceramics are doped with a high concentration of La^{3+}, $x \geq 0.03$, some extra peaks can be observed. This extra peaks can be assigned to the secondary phase $K_6Nb_{10.88}NbO_{30}$ (PDF#01-070-5051) that exhibits tetragonal tungsten-bronze (TTB) type structure. Zuo et al.[23] and Gao et al. [28] reported the absence of secondary phases using lower lanthanum amounts in La^{3+} doped KNN ceramics, although the occurrence of a small amount of this secondary phase cannot be discarded. The different results obtained could be explained by the slight different treatment of the precursor reagents, different processing procedures or the use of different powder precursors. Therefore, our results suggest that taking special care of the reagents and of the synthesis method plays an important role to avoid the formation of secondary phases, even at high amounts of dopants. An enlargement of the XRD patterns in the 2θ range from 23.5 ° to 29.0 ° of the KNN:xLa is shown in Fig. 1(b), which corresponds to the most relevant diffraction peaks of the TTB secondary phase. In KNN ceramics, the formation of the TTB secondary phase can be attributed to the volatilization of the

alkaline metals, especially Na^{+}, during sintering [29,30]. In our case, doping with large amounts of La^{3+} could destabilize the perovskite structure and enhance the volatilization of Na^{+} promoting the formation of the TTB phase. As a result, some alkaline deficiency is also expected for the ceramics with high content of La^{3+} since the TTB contains such ions. Fig. 1(b) also shows a magnification of the XRD patterns in the 2θ range from 43.5 ° to 47.0 ° of the KNN:xLa, in order to check the evolution of the (200) and (022) orthorhombic peaks. For the ceramics with x≤0.01 the splitting of the (200) and (022) peaks indicates the formation of an orthorhombic structure, while for higher La^{3+} content (x≥0.03) the peaks appear broadened and tend to merge to a single peak. This behaviour could be related with an increase of the composition heterogeneity. Probably due to the volatilization of the alkaline metals and the formation of the TTB phase but, could also be related with a decrease of the grain size when increasing the amount of La^{3+}.

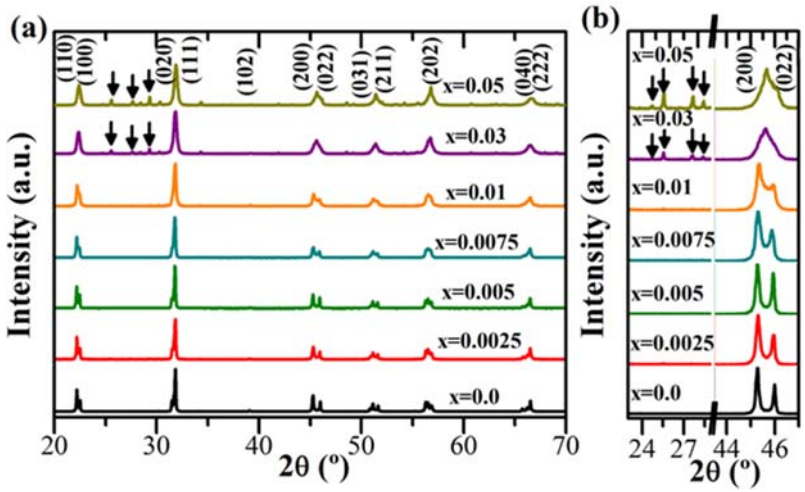

Figure 1: (a) XRD patterns corresponding to KNN:xLa ceramics. (b) Magnified XRD patterns in the 2θ ranges from 23.5 ° to 29.0 °, and from 43.5 ° to 47.0 ° of the KNN:xLa ceramics.

XRD patterns of all the prepared ceramics are refined using an orthorhombic symmetry with space group *Amm2* as expected for KNN-based ceramics [31]. Fig. 2(a) shows the evolution of the lattice parameters as a function of the La^{3+} amount. For low content of La^{3+}, x≤0.01, the lattice parameters slightly increase with respect to pure KNN, suggesting that the La^{3+}-addition does not modify drastically the crystalline structure. This behaviour together with the absence of

This is the post-print (i.e. final draft post-refereeing) of the publication.
The final publication is available at Elsevier via http://dx.doi.org/10.1016/j.ceramint.2016.08.066

secondary phases suggests that La^{3+} has diffused into the KNN lattice to form a solid solution. However, when increasing the La^{3+} content, cell volume decreases drastically and the amount of the TTB phase increases. To sum up, the addition of high contents of dopants slightly modifies the crystal structure, and promotes the formation of the TTB. The ionic radii of La^{3+} (1.03 Å) is very close to Na^{+} (1.02 Å) and smaller than K^{+} (1.38 Å) [32], thus, at high content of dopant, it cannot be discarded that La^{3+} may enter in substitution of Na^{+} and K^{+} substitution. This effect could promote the volatilization of Na^{+} and thus, promoting the formation of the K^{+} rich secondary phase.

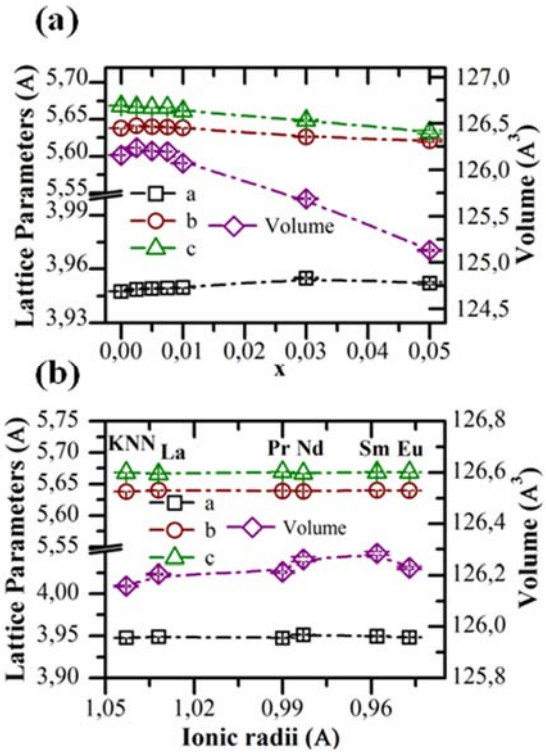

Figure 2: (a) Evolution of the lattice parameters of the KNN:xLa as a function of the La^{3+} content. (b) Evolution of the lattice parameters of the KNN:Ln as a function of the ionic radii of the lanthanide.

The XRD patterns of the ceramics when doping with different lanthanides and maintaining the same concentration (x=0.005) do not show a significant displacement of the diffraction peaks with respect to pure KNN. This behaviour and the absence of the secondary phases indicate that

This is the post-print (i.e. final draft post-refereeing) of the publication.
The final publication is available at Elsevier via http://dx.doi.org/10.1016/j.ceramint.2016.08.066

the different lanthanides diffuse into the KNN lattice forming a solid solution. The ionic radii of the lanthanides, La^{3+} (1.03 Å), Pr^{3+} (0.99 Å), Nd^{3+} (0.98 Å), Sm^{3+} (0.96 Å), Eu^{3+} (0.95 Å) [32], are slightly smaller than those of the alkaline metals, thus a decrease of the lattice parameters should be expected. However, as shown in Fig. 2(b), the lattice parameters vary less than 0.5 %, indicating that the structure does not change significantly upon doping.

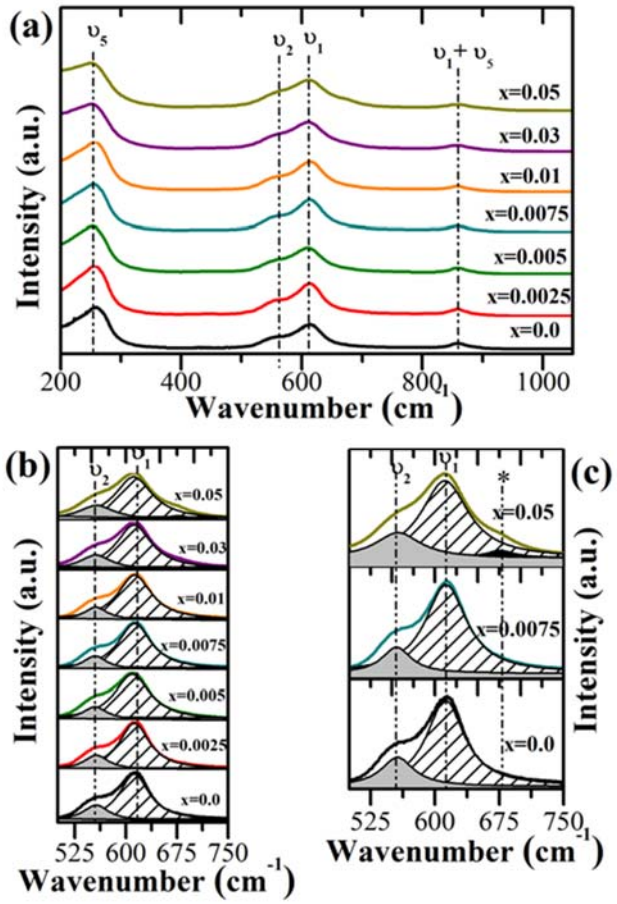

Figure 3: (a) Raman spectra of KNN:xLa ceramics. (b) Magnified Raman spectra in the wavenumber range from 500 to 750 cm^{-1} as a function of the composition and Lorentzian fits of the individual peaks of E_g (υ_2) and A_{1g} (υ_1) Raman modes. (c) Magnified Raman spectra in the 500 to 750 cm^{-1} region of the pure KNN, KNN:0.0075La and KNN:0.05La ceramics. The asterisk shows the appearance of the secondary phase peak.

The Raman spectra of the KNN:xLa (x = 0.0-0.05) sintered samples present the typical vibrations corresponding to a perovskite phase [33], as shown in Fig. 3 (a). A detail of the region between 500 and 700 cm^{-1} is presented in Fig. 3 (b). These spectra are fitted to the sum of two Lorentzian peaks, in all cases a correlation higher than 0.99 was obtained. The A_{1g} (ν_1)

This is the post-print (i.e. final draft post-refereeing) of the publication.
The final publication is available at Elsevier via http://dx.doi.org/10.1016/j.ceramint.2016.08.066

and E_g (ν_2) modes correspond to a symmetrical and asymmetrical vibration modes of the NbO_6 octahedra. The characteristic bands do not change significantly upon doping, except at high content of La^{3+} ($x \geq 0.03$), where the E_g (ν_2) band broadens and an additional peak appears at ~ 675 cm^{-1}, Fig. 3 (c). The appearance of a new band at higher wavenumbers can be associated with the formation of the TTB secondary phase, as has already been observed with tetragonal tungsten-bronze type structure materials, isostructural to $K_6Nb_{10.88}NbO_{30}$ [34,35].

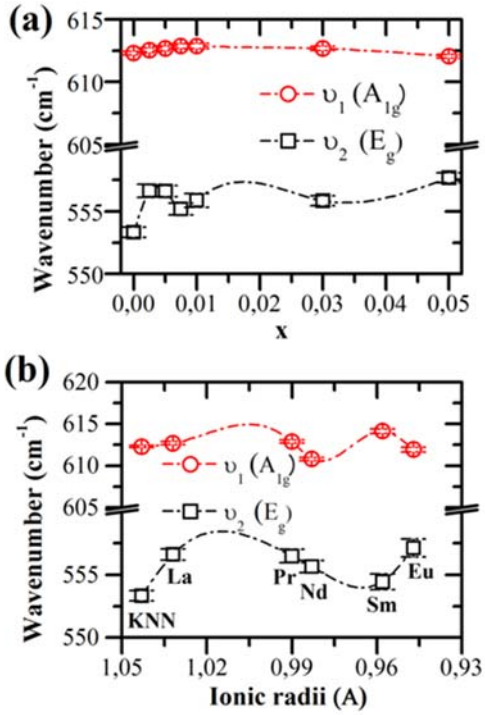

Figure 4: (a) Evolution of Raman shift of the E_g (υ_2) and A_{1g} (υ_1) Raman modes of the KNN:xLa ceramics as a function of the La^{3+} content, and (b) KNN:Ln as a function of the ionic radii of the lanthanide. Lines are guide to the eye only.

Analyzing in more detail the A_{1g} (ν_1) and E_g (ν_2) vibration modes of the KNN:xLa samples, the A_{1g} (ν_1) peaks do not show a shift in the wavenumber when doping, meanwhile, the E_g (ν_2) peaks shift to higher wavenumbers, Fig. 4(a). The shift to higher wavenumber can be related to an increase in the force constant between the Nb^{5+} ions and the coordinated oxygens and to an increase of the structural disorder provoked by the generation of cationic vacancies when doping with La^{3+} [36]. As can be observed, the E_g (ν_2) peaks shifts do not show a clear tendency when increasing the La^{3+} content. The same behaviour is observed when doping with

different lanthanides, Fig. 4(b), where the A_{1g} (ν_1) peaks remain practically constant, while the E_g (ν_2) peaks shift to higher wavenumbers, although there is no clear tendency as a function of the ionic radii of the lanthanides.

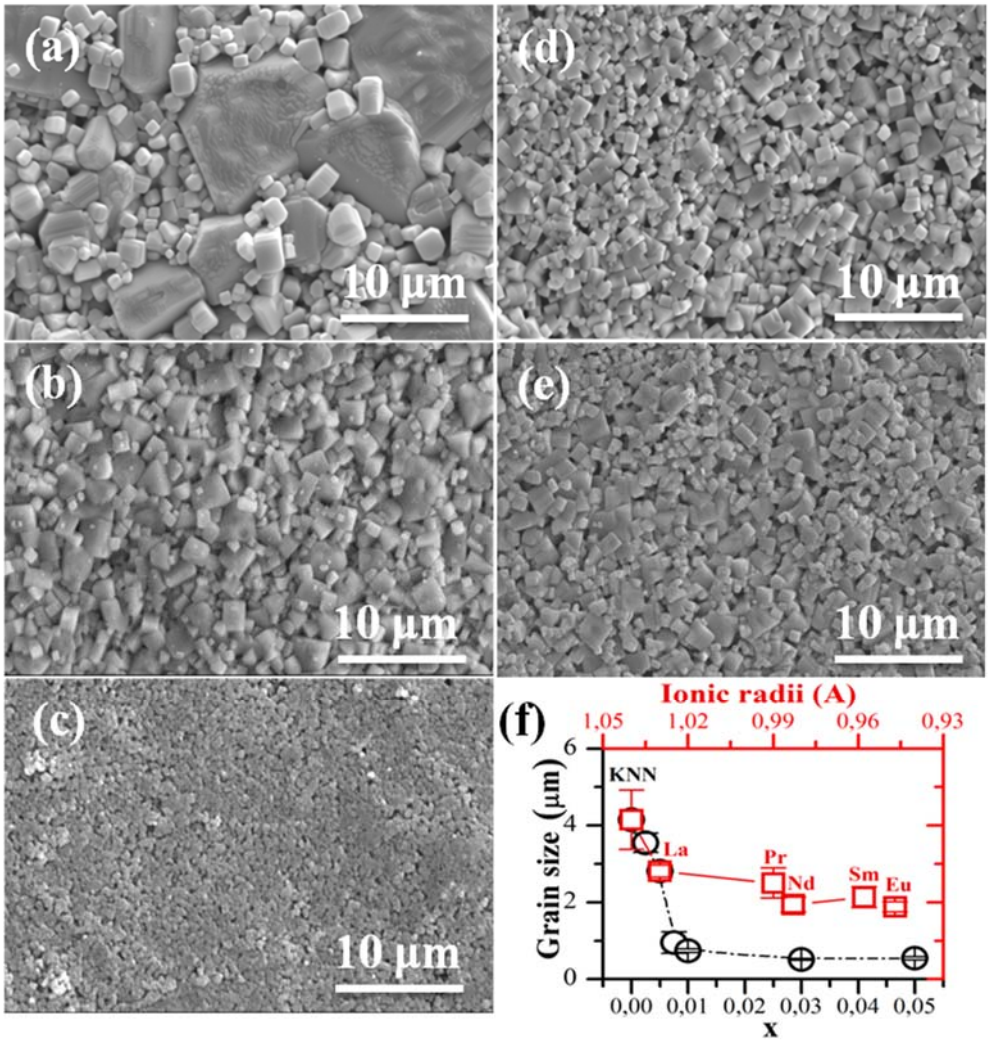

Figure 5: Microstructure of (a) pure KNN, (b) KNN:0.005La, (c) KNN:0.05La, (d) KNN:Pr, (e) KNN:Eu ceramics and (f) evolution of the grain size of the KNN:xLa and KNN:Ln ceramics as a function of the La^{3+} content and the ionic radii of the lanthanide respectively. Lines are guide to the eye only

3.2. *Microstructural characterization*

The FE-SEM images of the KNN:xLa with x = 0.0, 0.005 and 0.05, and KNN:Ln with Ln= Pr and Eu are respectively show in Fig. 5(a-e). All micrographs show the typical morphology of the alkaline niobate ceramics with cube-like shape grains. For pure KNN, Fig. 5(a), the surface reveals the presence of some large abnormal grains, with a grain size higher than 10 µm, and at the same time small grains of about 500 nm. A change of the average grain size is observed with

La^{3+} content, as depicted in Fig. 5(b and c). As the content of La^{3+} increases, the grain size decreases significantly, and moreover, at high content of dopant (x>0.0075) the grain size decreases drastically reaching values of grain size lower than 500 nm when x = 0.05, Fig. 5(f). When doping with different lanthanides, a similar behaviour is observed, i.e. a decrease of the grain size, Fig. 5(d and e). In addition, there exists a slight tendency of the grain size as a function of the ionic radii of the introduced lanthanide, as can be seen in Fig. 5(f). The smaller the ionic radii, the smaller the grain size. To sum up, donor dopant inhibits the grain growth as already observed for other La-doped KNN [28] and other La-doped perovskite-type ceramics [20,37,38] ceramics. Donor dopants usually inhibit the grain growth as observed in PZT-based ceramics by reducing the diffusion coefficient since A-site vacancies created by doping are supposed to be bound to the doping ion [39]. As observed in our case, the lanthanide concentration has a greater effect by reducing the grain size than the type of lanthanide itself.

The HRTEM image of the KNN:xLa with x = 0.005 is displayed in Fig. 6 (a). The experimental image taken along the [011] axis shows excellent agreement with the simulated images depicted within the rectangle marked with (yellow) asterisks. In these experimental conditions, the black dots correspond to Nb atoms, while the less intense dots correspond to Na^{+}, K^{+} and La^{3+} cations, as represented in Fig 6. (b). The image shows a well-ordered crystal without the formation of superstructures or defects. This is evidenced by a regular contrast across the HRTEM image and the absence of extra spots or streaking lines in the FFTs (Fig. 6 (a) inset). In the image we can directly measure the *a* and *c* cell parameters, which correspond to 3.9 and 5.6 Å consistent with those measured by XRD. On the left side of the calculated image a sketch of the structure with the octahedral NbO_6 coloured in green and the alkaline and lanthanum cations, in white/purple matches perfectly with the dark dots. Selected Area Electron Diffraction (SAED) patterns along the [011] and [010] corresponding to a KNN:xLa with x = 0.005 crystal are shown in Fig. 6 (c) and (d). The obtained diagrams were indexed with an orthorhombic *Amm2* structure, using the cell parameters obtained by XRD. The results do not show any evidence of superstructures due

to La^{3+} doping, and there is no presence of secondary phases between grains, and thus, the formation of a single phase is confirmed.

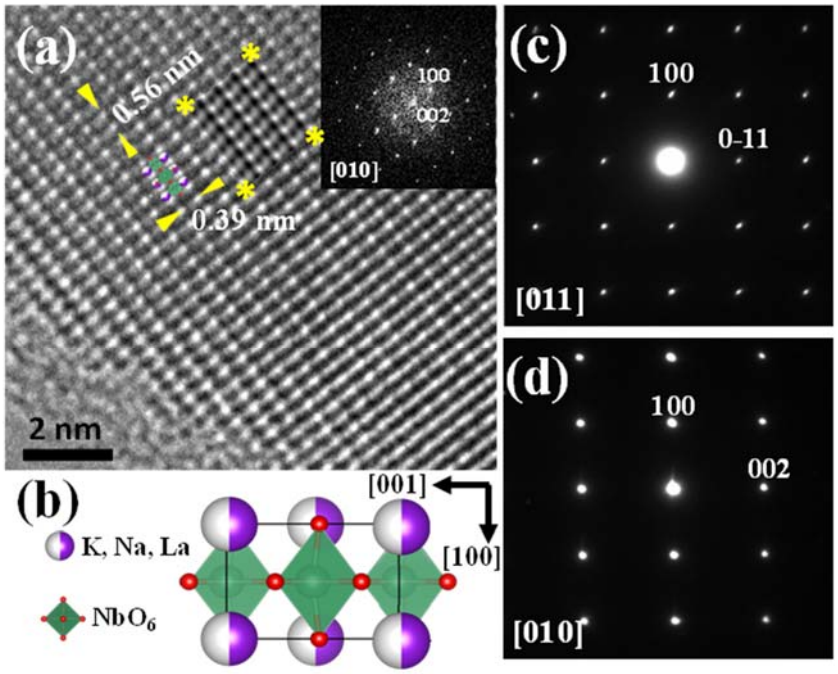

Figure 6: (a) HRTEM image from a thin crystal of KNN:0.005La ceramic along the [010] axis with the corresponding Fourier Transform and a superposed simulated image, shown between the rectangle marked with asterisks. (b) Projection of the cell along the [010] axis. (c) and (d) SAED patterns along the zone axes [011] and [010] of KNN:0.005La.

3.3. Dielectric properties

The temperature dependence of the real part of the relative permittivity of KNN:xLa and KNN:Ln ceramics, measured at 10 kHz from RT to 450 ºC is shown in Fig. 7. In all cases, permittivity versus temperature shows two anomalies, one at around 200 ºC corresponding to orthorhombic-tetragonal ($T_{O\text{-}T}$) phase transition, and the other at higher temperatures, around 350-420 ºC, corresponding to the tetragonal-cubic (T_C) phase transition. In KNN:xLa ceramics, Fig. 7 (a), the T_C remains sharp and well defined, but when increasing the La^{3+} concentration ($x \geq 0.03$) the maximum broadens and cannot be distinguish accurately. On the other hand, KNN:Ln ceramics do not show a broadening of the maximum, but it is displaced towards lower temperature with respect to pure KNN, Fig. 7 (b).

This is the post-print (i.e. final draft post-refereeing) of the publication.
The final publication is available at Elsevier via http://dx.doi.org/10.1016/j.ceramint.2016.08.066

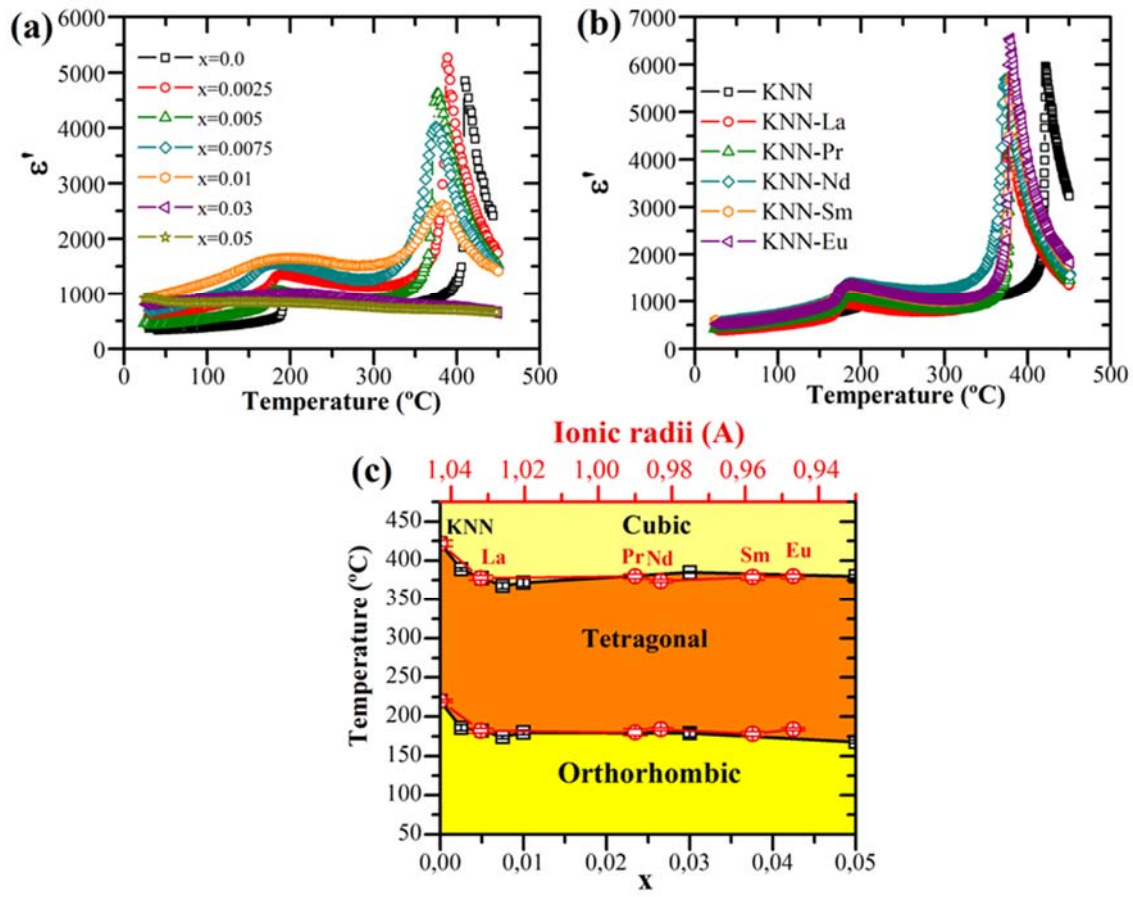

Figure 7: Temperature dependence of the real part of the relative permittivity of KNN:xLa (a) and KNN:Ln (b) ceramics. (c) Evolution of the orthorhombic-tetragonal (T_{O-T}) and tetragonal-cubic (T_C) phase transitions as a function of the lanthanum content and the ionic radii of the lanthanide.

The broadening of the maximum suggests a deviation of the Curie-Weiss law, where a diffuse phase transition is induced and the ceramics transforms gradually from a 'normal' to a diffuse phase transition when increasing the La^{3+} content. Therefore, the diffuseness coefficient (γ) of the phase transition can be determined from the modified Curie-Weiss law $1/\varepsilon_r - 1/\varepsilon_m = C^{-1}(T-T_m)^{\gamma}$ [40], where $\gamma=2$ corresponds to a completely diffuse phase transition and $\gamma=1$ corresponds to a 'normal' ferroelectric-paraelectric phase transition [41]. As shown in Table 1, when increasing the La^{3+} content, ceramics show an increase of the diffuseness, thus a diffuse phase transition is obtained when increasing the La^{3+} content. Similar behaviour has been already observed in La-doped KNN ceramics [23,28], Cu-doped KNN ceramics [42] and in Nb-doped PZT-based ceramics [43,44]. This effect could be attributed to an increase of the structural disorder caused

This is the post-print (i.e. final draft post-refereeing) of the publication.
The final publication is available at Elsevier via http://dx.doi.org/10.1016/j.ceramint.2016.08.066

by the introduction of La^{3+} into the KNN structure and the subsequent formation of cationic vacancies. Furthermore, as mentioned above, when doping with large amounts of La^{3+} the formation of the TTB phase is promoted due to alkaline metals volatilization and, as a consequence a diffuse phase transition can also be attributed to a microscopic compositional fluctuation [45]. However, when adding the same concentration of different lanthanides, the diffuseness is maintained practically unchanged as function of the lanthanide. Thus, when doping pure KNN with lanthanides, their concentration has a greater effect on the dielectric properties than the type of lanthanide. This effect can also be observed in Fig. 7 (c), where the phase transition temperatures of all the prepared KNN-based ceramics are displayed as a function of the ionic radii of the lanthanide or the lanthanum concentration. A decrease in temperature can be observed in both phase transitions when doping, independently of the lanthanide. However, a dependence of the lanthanum concentration with temperature is observed at low doping concentration ($x<0.01$), but at higher concentration the phase transition temperatures are maintained practically constant. This effect could be attributed to the limited solubility of lanthanum in the KNN structure.

Table 1: Dieletric and piezoelectric properties of KNN:xLa and KNN:Ln ceramics at room temperature. The diffuseness coeffiecient γ is also reported.

	La							Pr	Nd	Sm	Eu
x	0	0.0025	0.005	0.0075	0.01	0.03	0.05	0.005	0.005	0.005	0.005
ε' (10 kHz)	338	582	642	693	902	802	890	572	603	597	584
tanδ (10 kHz)	0.061	0.052	0.058	0.074	0.082	0.166	0.351	0.054	0.047	0.043	0.045
- d_{31} (pC/N)	19	21	24	24	-	-	-	21	22	25	26
k_p (%)	28.6	29.3	31.5	33.7	-	-	-	26.4	27.5	31.6	33.2
d_{33} (pC/N)	96	100	110	118	-	-	-	108	115	120	124
γ	1.18	1.28	1.45	1.68	1.75	1.82	1.88	1.38	1.26	1.24	1.18

3.4. Ferroelectric and piezoelectric properties

The ferroelectric hysteresis loops for the KNN:xLa and KNN:Ln ceramics measured at 1Hz and at room temperature are shown in Fig. 8(a, b). In KNN:xLa ceramics, a slight increase of the remanent polarization (P_r) and coercitive field (E_C) is observed when increasing the La^{3+} concentration. However, due to the high conductivity observed when doping with large amounts of La^{3+}, only the KNN-doped ceramics with low lanthanum content ($x \leq 0.0075$) show the typical hysteresis loops of a ferroelectric material. This effect can be attributed to the high dielectric losses observed when doping with high content of La^{3+} (Table 1), and to the formation of the TTB secondary phase, as discussed above. Meanwhile, in KNN-Ln ceramics, a strongly increase of the remanent polarization is observed in all cases, from 17.1 $\mu C/cm^2$ for pure KNN to 32.4 $\mu C/cm^2$ for Pr-doped KNN. This variation can be observed in Fig. 8 (c), where the values of P_r are represented as a function of the concentration of La^{3+} and the ionic radii of the lanthanide. As can be seen, the type of lanthanide plays an important role on the ferroelectric properties of KNN-based ceramics instead of its concentration. The increase of the remanent polarization can be related with the donor doping, as has already been described in similar perovskite-type ceramics [20,46,47]. A slight increase of the coercitive field observed in all cases may be attributed to the sub-micrometre grains obtained in the prepared doped ceramics.

Piezoelectric constants (d_{33} and d_{31}) and electromechanical coupling factor (k_p) as a function of the La^{3+} content and of the lanthanide are shown Table 1. As mentioned above, high conductivity is observed at high content of La^{3+}, thus, the piezoelectric and electromechanical properties of high La^{3+} content ceramics ($x>0.01$) could not be measured. In all cases, an increase of the piezoelectric and electromechanical properties is observed with respect to pure KNN, which is in agreement with the introduction of donor dopants. A slight tendency can also be observed as a function of the ionic radii of the lanthanide, the smaller the ionic radii, the higher the piezoelectric and electromechanical properties. Therefore, the Eu^{3+} doped ceramics show higher d_{33}, d_{31} and k_p values. It should also be noted that the piezoelectric properties tend to decline when abnormal grains appear [48], as in the case of pure KNN (Fig. 5), whereas,

when doping a uniform grain growth is obtained and higher piezoelectric properties are obtained.

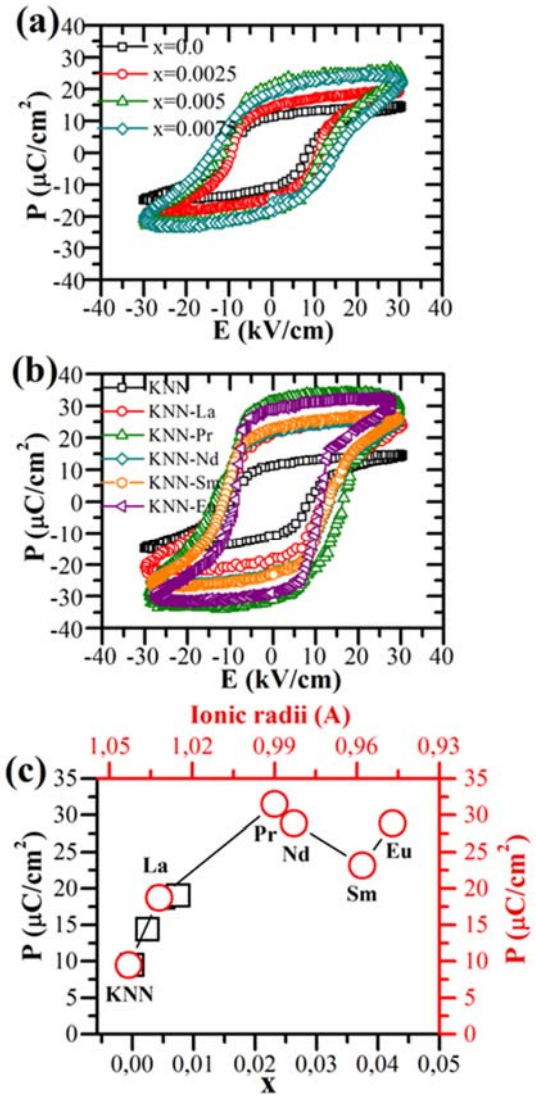

Figure 8: P-E hysteresis loops of the KNN:xLa (a) and KNN:Ln (b) ceramics measured at room temperature and at 1 Hz. (c) Evolution of the remanent polarization of the KNN:xLa and KNN:Ln ceramics.

4. Conclusions

$(K_{0.5}Na_{0.5})_{1-3x}La_xNbO_3$ (x = 0.0- 0.05) and $(K_{0.5}Na_{0.5})_{1-3x}Ln_xNbO_3$ x=0.005 being Ln = La, Pr, Nd, Sm and Eu, ceramics have been prepared by conventional solid-state reaction. The special care of the reagents, prior to solid-state reaction synthesis and during the whole synthesis process assures the formation of a single phase, even at high amounts of donor dopants. However, the

TTB phase is promoted at high content of dopants, which significantly deteriorates the functional properties of the ceramics by increasing the dielectric losses. As expected, donor dopants inhibit the grain growth and show a slight tendency as a function of the ionic radii of the lanthanide, the smaller the ionic radii, the smaller the grain size. Finally, the donor doping effect on KNN ceramics depends as much on type of dopant (lanthanides) as on their concentration. The piezoelectric and ferroelectric properties are greatly enhanced when doping with small concentrations of lanthanides, and show a tendency as a function of the ionic radii of the lanthanide, the lower ionic radii the better ferroelectric and piezoelectric properties are. This feature will be investigated in more detail to gain a better understanding of these effects. It should be noted that with low donor doping amounts, the main grain size, dielectric, ferroelectric and piezoelectric properties of KNN can be modified greatly. Therefore, donor dopants could not be discarded to improve the functional properties of KNN-based piezoceramics, by a decrease of the losses and increasing the dielectric constant, the piezoelectric coefficients and the coupling factor.

Acknowledgements

The authors acknowledge technical support from Prof. Emilio Morán and Dr. David Ávila-Brande with HRTEM measurements. The authors would also like to thank the MINECO (Spanish Government) project MAT2013-48009-C4-P.

References

[1] N. Setter, Piezoelectric materials in devices : extended reviews on current and emerging piezoelectric materials technology, and applications, EPFL, Lausanne, 2003.
[2] M.S. Bhuiyan, M. Paranthaman, K. Salama, Solution-derived textured oxide thin films—a review, Supercond. Sci. Technol. 19 (2006) R1–R21. doi:10.1088/0953-2048/19/2/R01.
[3] B. Jaffe, W.R. Cook, H. Jaffe, Piezoelectric ceramics, Academic Press: London, New York, 1971.
[4] S. Sharma, V. Sharma, R. Paliwal, Pracheta, Lead toxicity, oxidative damage and health implications. A review, Int. J. Biotechnol. Mol. Biol. Res. 2 (2011) 215–221. doi:10.5897/IJBMBRX11.002.
[5] M. Shahid, E. Pinelli, C. Dumat, Review of Pb availability and toxicity to plants in relation with metal speciation; role of synthetic and natural organic ligands., J. Hazard. Mater. 219-220 (2012) 1–12. doi:10.1016/j.jhazmat.2012.01.060.

[6] EU-Directive 2002/95/EC: Restriction of the use of certain hazardous substances in electrical and electronic equipment (RoHS), Off. J. Eur. Union. 46 (2003) 19.
[7] T.R. Shrout, S.J. Zhang, Lead-free piezoelectric ceramics: Alternatives for PZT?, J. Electroceramics. 19 (2007) 113–126. doi:10.1007/s10832-007-9047-0.
[8] M.D. Maeder, D. Damjanovic, N. Setter, Lead Free Piezoelectric Materials, J. Electroceramics. 13 (2004) 385–392. doi:10.1007/s10832-004-5130-y.
[9] J. Rödel, K.G. Webber, R. Dittmer, W. Jo, M. Kimura, D. Damjanovic, Transferring lead-free piezoelectric ceramics into application, J. Eur. Ceram. Soc. 35 (2015) 1659–1681. doi:10.1016/j.jeurceramsoc.2014.12.013.
[10] Y. Saito, H. Takao, T. Tani, T. Nonoyama, K. Takatori, T. Homma, et al., Lead-free piezoceramics, Nature. 432 (2004) 84.
[11] D. Lin, K.W. Kwok, H.L.W. Chan, Piezoelectric and ferroelectric properties of Cu-doped $K_{0.5}Na_{0.5}NbO_3$ lead-free ceramics, J. Phys. D. Appl. Phys. 41 (2008) 045401. doi:10.1088/0022-3727/41/4/045401.
[12] M.R. Saeri, A. Barzegar, H. Ahmadi Moghadam, Investigation of nano particle additives on lithium doped KNN lead free piezoelectric ceramics, Ceram. Int. 37 (2011) 3083–3087. doi:10.1016/j.ceramint.2011.05.044.
[13] Z. Li, G. Xu, Y. Li, A. Sun, L. Duan, J. Jiang, et al., Dielectric and piezoelectric properties of ZnO and SnO_2 co-doping $K_{0.5}Na_{0.5}NbO_3$ ceramics, Phys. B Condens. Matter. 405 (2010) 296–299. doi:10.1016/j.physb.2009.08.080.
[14] I.-Y. Kang, I.-T. Seo, Y.-J. Cha, J.-H. Choi, S. Nahm, T.-H. Sung, et al., Low temperature sintering of ZnO and MnO_2-added $(Na_{0.5}K_{0.5})NbO_3$ ceramics, J. Eur. Ceram. Soc. 32 (2012) 2381–2387. doi:10.1016/j.jeurceramsoc.2012.01.030.
[15] F. Rubio-Marcos, J.J. Romero, M.G. Navarro-Rojero, J.F. Fernandez, Effect of ZnO on the structure, microstructure and electrical properties of KNN-modified piezoceramics, J. Eur. Ceram. Soc. 29 (2009) 3045–3052. doi:10.1016/j.jeurceramsoc.2009.04.026.
[16] X. Vendrell, J.E. García, X. Bril, D. A. Ochoa, L. Mestres, G. Dezanneau, Improving the functional properties of $(K_{0.5}Na_{0.5})NbO_3$ piezoceramics by acceptor doping, J. Eur. Ceram. Soc. 35 (2015) 125–130. doi:10.1016/j.jeurceramsoc.2014.08.033.
[17] G.H. Haertling, Ferroelectric Ceramics: History and Technology, J. Am. Ceram. Soc. 82 (1999) 797–818. doi:10.1111/j.1151-2916.1999.tb01840.x.
[18] J. Taub, L. Ramajo, M.S. Castro, Phase structure and piezoelectric properties of Ca- and Ba-doped $K_{1/2}Na_{1/2}NbO_3$ lead-free ceramics, Ceram. Int. 39 (2013) 3555–3561. doi:10.1016/j.ceramint.2012.10.181.
[19] A. R. James, J. Subrahmanyam, Processing and structure-property relation of fine-grained PLZT ceramics derived from mechanochemical synthesis, J. Mater. Sci. Mater. Electron. 17 (2006) 529–535. doi:10.1007/s10854-006-8236-y.
[20] X. Diez-Betriu, J.E. Garcia, C. Ostos, A. U. Boya, D. A. Ochoa, L. Mestres, et al., Phase transition characteristics and dielectric properties of rare-earth (La, Pr, Nd, Gd) doped $Ba(Zr_{0.09}Ti_{0.91})O_3$ ceramics, Mater. Chem. Phys. 125 (2011) 493–499. doi:10.1016/j.matchemphys.2010.10.027.
[21] D. Gao, K.W. Kwok, D. Lin, H.L.W. Chan, Microstructure, electrical properties of CeO_2-doped $(K_{0.5}Na_{0.5})NbO_3$ lead-free piezoelectric ceramics, J. Mater. Sci. 44 (2009) 2466–2470. doi:10.1007/s10853-009-3314-1.
[22] J. Fuentes, J. Portelles, A. Pérez, M.D. Durruthy-Rodríguez, C. Ostos, O. Raymond, et al., Structural and dielectric properties of La- and Ti-modified $K_{0.5}Na_{0.5}NbO_3$ ceramics, Appl. Phys. A. 107 (2012) 733–738. doi:10.1007/s00339-012-6793-x.
[23] R. Zuo, M. Wang, B. Ma, J. Fu, T. Li, Sintering and electrical properties of $Na_{0.5}K_{0.5}NbO_3$ ceramics modified with lanthanum and iron oxides, J. Phys. Chem. Solids. 70 (2009) 750–754. doi:10.1016/j.jpcs.2009.03.003.
[24] H. Sun, D. Peng, X. Wang, M. Tang, Q. Zhang, X. Yao, Green and red emission for $(K_{0.5}Na_{0.5})NbO_3$:Pr ceramics, J. Appl. Phys. 111 (2012) 046102. doi:10.1063/1.3686193.
[25] J. Rodriguez-Carvajal, Recent advances in magnetic structure determination by neutron powder diffraction, Phys. B Condens. Matter. 192 (1993) 55.
[26] Digital Micrograph software 1.71.38 Gatan Inc.

[27] MacTempas Software, (Version 2.3.7, Roar Kilaas).
[28] D. Gao, K.W. Kwok, D. Lin, H.L.W. Chan, Microstructure and electrical properties of La-modified $K_{0.5}Na_{0.5}NbO_3$ lead-free piezoelectric ceramics, J. Phys. D. Appl. Phys. 42 (2009) 035411. doi:10.1088/0022-3727/42/3/035411.
[29] Y. Zhen, J.-F. Li, Normal Sintering of (K,Na)NbO_3 -Based Ceramics: Influence of Sintering Temperature on Densification, Microstructure, and Electrical Properties, J. Am. Ceram. Soc. 89 (2006) 3669–3675. doi:10.1111/j.1551-2916.2006.01313.x.
[30] Y. Wang, D. Damjanovic, N. Klein, N. Setter, High-Temperature Instability of Li- and Ta-Modified (K,Na)NbO_3 Piezoceramics, J. Am. Ceram. Soc. 91 (2008) 1962–1970. doi:10.1111/j.1551-2916.2008.02392.x.
[31] D.W. Baker, P. A. Thomas, N. Zhang, A. M. Glazer, A comprehensive study of the phase diagram of $K_xNa_{1-x}NbO_3$, Appl. Phys. Lett. 95 (2009) 091903. doi:10.1063/1.3212861.
[32] R.D. Shannon, Revised Effective Ionic Radii and Systematic Studies of Interatomie Distances in Halides and Chaleogenides, Acta Crystallogr. A32 (1976) 751–767.
[33] K. Kakimoto, K. Akao, Y. Guo, H. Ohsato, Raman Scattering Study of Piezoelectric $(Na_{0.5}K_{0.5})NbO_3$-$LiNbO_3$ Ceramics, Jpn. J. Appl. Phys. 44 (2005) 7064–7067. doi:10.1143/JJAP.44.7064.
[34] T. Debnath, S.C. Roy, C.H. Rüscher, A. Hussain, Synthesis and characterization of niobium-doped potassium tetragonal tungsten bronzes, $K_xNb_yW_{1-y}O_3$, J. Mater. Sci. 44 (2008) 179–185. doi:10.1007/s10853-008-3101-4.
[35] C.L. Mak, B. Lai, K.H. Wong, Fabrication and Characterization of Sol-Gel Derived Potassium Sodium Strontium Barium Niobate, J. Sol-Gel Sci. Technol. 18 (2000) 225–233.
[36] F. HARDCASTLE, I. WACHS, Determination of niobium-oxygen bond distances and bond orders by Raman spectroscopy, Solid State Ionics. 45 (1991) 201–213. doi:10.1016/0167-2738(91)90153-3.
[37] H.-D. Li, C.-D. Feng, P.-H. Xiang, Electrical Properties of La^{3+}-Doped $(Na_{0.5}Bi_{0.5})_{0.94}Ba_{0.06}TiO_3$ Ceramics, Jpn. J. Appl. Phys. 42 (2003) 7387–7391. doi:10.1143/JJAP.42.7387.
[38] M.D. Durruthy-Rodríguez, L.D. Pérez-Fernández, A. Peláiz-Barranco, F. Calderón-Piñar, Structural and dielectric characteristics of donor dopants in A and B places of perovskite ceramic PZT 54/46, Appl. Phys. A. 95 (2008) 423–428. doi:10.1007/s00339-008-4889-0.
[39] C. Moure, M. Villegas, J.F. Fernández, P. Durán, Microstructural and piezoelectric properties of fine grained PZT ceramics doped with donor and/or acceptor cations, Ferroelectrics. 127 (1992) 113–118. doi:10.1080/00150199208223356.
[40] K. Uchino, S. Nomura, Critical exponents of the dielectric constants in diffused-phase-transition crystals, Ferroelectrics. 44 (2011) 55–61. doi:10.1080/00150198208260644.
[41] G.A. Smolenskii, Physical phenomena in ferroelectric with diffused phase transition, J. Phys. Soc. Japan. 28 supplem (1970) 26–37.
[42] F. Rubio-Marcos, J.J. Reinosa, X. Vendrell, J.J. Romero, L. Mestres, P. Leret, et al., Structure, microstructure and electrical properties of Cu^{2+} doped (K,Na,Li)(Nb,Ta,Sb)O_3 piezoelectric ceramics, Ceram. Int. 39 (2013) 4139–4149. doi:10.1016/j.ceramint.2012.10.270.
[43] X. Zeng, A. L. Ding, G.C. Deng, T. Liu, X.S. Zheng, Effects of lanthanum doping on the dielectric, piezoelectric properties and defect mechanism of PZN-PZT ceramics prepared by hot pressing, Phys. Status Solidi. 202 (2005) 1854–1861. doi:10.1002/pssa.200420049.
[44] M. Adamczyk, Z. Ujma, L. Szymczak, I. Gruszka, Effect of Nb doping on the relaxor behaviour of $(Pb_{0.75}Ba_{0.25})(Zr_{0.70}Ti_{0.30})O_3$ ceramics, J. Eur. Ceram. Soc. 26 (2006) 331–336. doi:10.1016/j.jeurceramsoc.2004.11.002.
[45] F. Rubio-Marcos, P. Marchet, T. Merle-Méjean, J.F. Fernandez, Role of sintering time, crystalline phases and symmetry in the piezoelectric properties of lead-free KNN-modified ceramics, Mater. Chem. Phys. 123 (2010) 91–97.

doi:10.1016/j.matchemphys.2010.03.065.

[46] M.D. Durruthy-Rodríguez, L.D. Pérez-Fernández, A. Peláiz-Barranco, F. Calderón-Piñar, Structural and dielectric characteristics of donor dopants in A and B places of perovskite ceramic PZT 54/46, Appl. Phys. A. 95 (2008) 423–428. doi:10.1007/s00339-008-4889-0.

[47] X.X. Wang, H.L.W. Chan, C.L. Choy, $(Bi_{0.5}Na_{0.5})_{0.94}Ba_{0.06}TiO_3$ lead-free ceramics with simultaneous addition of CeO_2 and La_2O_3, Appl. Phys. A. 80 (2003) 333–336. doi:10.1007/s00339-003-2210-9.

[48] Y. Chang, Z. Yang, D. Ma, Z. Liu, Z. Wang, Phase transitional behavior, microstructure, and electrical properties in Ta-modified $[(K_{0.458}Na_{0.542})_{0.96}Li_{0.04}]$ NbO_3 lead-free piezoelectric ceramics, J. Appl. Phys. 104 (2008) 024109. doi:10.1063/1.2957591.